# Chapter 2
# Complex Behavior of VMC Buck Converter: Characterization

The previous chapter has reviewed trends in advanced power management architectures, considering different converters, controllers and functionalities, along with revisiting the available models to predict the dynamics of such architectures.

This chapter is focused on exploring and characterizing the different behaviors that can be exhibited in a switching power converter under a VMC in two ways. On the one hand the interest is centered on exploring the effect of the whole design parameter space parameters upon system dynamics by dividing the multidimensional design parameter space in different stability regions. On the other hand, it is focused on characterizing the dynamic behavior in such regions from specific power-oriented metrics in order to quantify whether or not they are of interest depending on the front-end application.

## 2.1 Design-Space Characterization of a Voltage-Mode Buck Converter

A switching power system is composed of different nature parameters, encompass those of the converter, controller and modulator.

This section is focused on characterizing the dynamic regimes in different regions of such parametric space starting from a VMC buck converter under a PI control and PWM modulator, shown in Fig. 2.1. The PI controller can be described in the frequency domain as:

$$G_c(s) = k_p \frac{s + \omega_{z1}}{s} \tag{2.1}$$

Considering this system, which is simple but representative of classical voltage-mode regulation, its complete design parameter space $W$ is 9-dimensional:

$$W := (V_g, V_{ref}, L, C, R, k_p, \omega_{z1}, V_m, f_s) \in \mathbb{R}^9 \tag{2.2}$$

E. Rodríguez Vilamitjana et al., *Chaos in Switching Converters for Power Management*,
DOI: 10.1007/978-1-4614-2128-3_2, © Springer Science+Business Media New York 2013

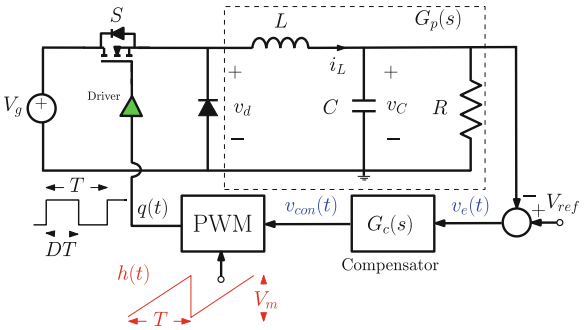


**Fig. 2.1** VMC buck converter with a control $G_c(s)$ and PWM modulator controller

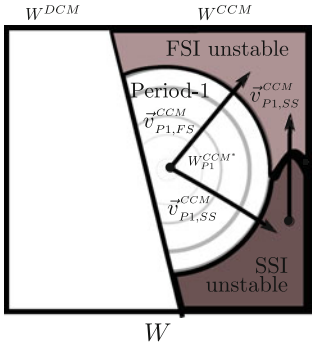


**Fig. 2.2** Descriptive working regions in CCM

where $V_g$ is the input voltage, $V_{ref}$ is the voltage reference, $L$ is the inductance, $C$ is the output capacitance, $R$ is the output resistance value, $k_p$ is the proportional gain, $\omega_{z1}$ is the zero of the PI compensator, $V_m$ is the PWM ramp amplitude and $f_s$ is the PWM ramp frequency (coinciding with the switching frequency in stable regime).

In switching power converters, the design parameter space $W$ can be categorically split into two regions since they can work in two different conduction modes which fundamentally alter the switching process and hence the resulting dynamics. The boundary between both modes is determined by the condition resulting in a null current at the end of the switching period. Boundary between both modes is well known, and, for a buck converter and assuming low-output ripple, it can be expressed as:

$$\frac{\overline{D}}{D} = \frac{2Lf_s}{R} \tag{2.3}$$

where $D$ is the duty cycle of the PWM signal and $\overline{D} = 1 - D$. The next sections are centered on characterizing the effect of the whole design parameter space upon the system dynamics and the boundaries between the different dynamical behavior.

### 2.1.1 Dynamics of a VMC Buck Converter Working in CCM

In general, the different kinds of dynamics that can be exhibited in a switching power converter can be classified according to their periodicity, as it was mentioned in Sect. 1.3.1: period-one, in which the system periodicity is the switching frequency, FSI, including period-doubling, subharmonic oscillations and chaotic behavior, and SSI, characterized by the exhibition of low-frequency oscillation.

A qualitative map, considering the whole CCM design parameter space $W^{\mathrm{CCM}}$ and the possible kinds of behaviors and the related trajectories among them $\mathbf{v}^{\mathrm{CCM}}$, is shown in Fig. 2.2. Note that within the generic FSI and SSI regions, each of them could be subdivided and consist of more complex behaviors, thus being possible to find different dynamics such as period-doubling, period-four, or chaotic behavior in the case of the FSI region.

The numerical characterization in Figs. 2.3, 2.4 and 2.5 show one-dimensional trajectories by sweeping one parameter of the design parameter space $W^{\mathrm{CCM}}$. Such dynamic routes are plotted by means of bifurcation diagrams, which consist of sampling one state variable at the switching frequency which allows to identify the periodicity of the behavior hence classifying it. The parameter values used in this chapter, corresponding to the starting point $W^{\mathrm{CCM}^*}$, are: $V_g = 6\,\mathrm{V}$, $V_{ref} = 3\,\mathrm{V}$, $R = 2.5\,\Omega$, $L = 66\,\mathrm{nH}$, $C = 20\,\mathrm{nF}$, $f_s = 50\,\mathrm{MHz}$, $V_m = 1\,\mathrm{V}$, $k_p = 3$ and $\omega_{z1} = 10\,\mathrm{Mrad/s}$. These values correspond to a miniaturized converter aiming on-chip integration (Villar and Alarcon 2008).

Note that the previous diagrams lead to exhibit different kinds of instabilities depending upon which parameter is swept.

Starting from a stable point in period-one (P1) within the CCM region $W_{\mathrm{P1}}^{\mathrm{CCM}^*}$, it is possible to define different routes depending upon the initial and final states. Observing the previous bifurcation diagrams, we can identify two possible routes: ending up in FSI region $\mathbf{v}_{\mathrm{P1,FS}}^{\mathrm{CCM}}$ or ending up within SSI region $\mathbf{v}_{\mathrm{P1,SS}}^{\mathrm{CCM}}$.

According to the previous nomenclature and with the previous simulation results, the routes starting from a stable period-one behavior within CCM region $W_{\mathrm{P1}}^{\mathrm{CCM}}$ can be split as:

$$\mathbf{v}_{\mathrm{P1,FS}}^{\mathrm{CCM}}(L, C, f_s, V_g, V_{ref}, k_p)$$
$$\mathbf{v}_{\mathrm{P1,SS}}^{\mathrm{CCM}}(R, C, \omega_{p1})$$

The routes shown in the bifurcation diagrams are only valid for the given starting point $W_{\mathrm{P1}}^{\mathrm{CCM}^*}$ and moving along one dimension, and hence they can not be considered univocal for the other points within $W^{\mathrm{CCM}}$. Therefore, it is considered an alternative exploration of such design parameter space in order to determine the possible routes. The exploration of the design parameter space pair $(k_p, \omega_{z1})$, which is shown in Fig. 2.6, unveils complex boundaries dependency of both parameter values.

Further exploration shows that other parameters can lead to both kinds of behavior depending upon the starting point. For instance, this occurs in the case of proportional

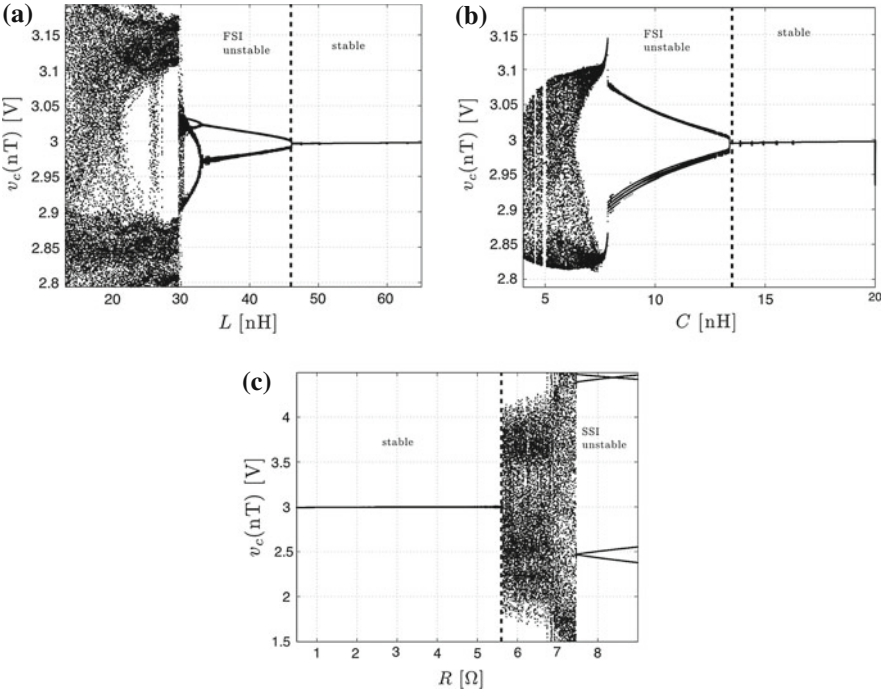


**Fig. 2.3** Bifurcation diagrams obtained by sweeping different converter parameters. **a**–**b** FSI, **c** SSI

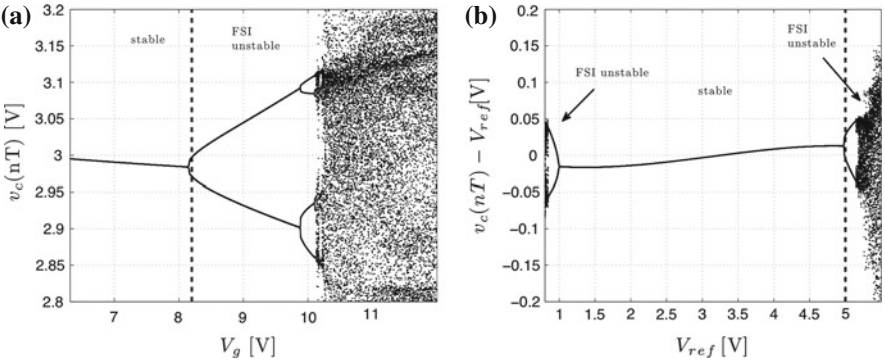


**Fig. 2.4** Bifurcation diagrams obtained by sweeping the input and the reference voltages $V_g$ and $V_{ref}$ respectively

gain $k_p$ or modulation amplitude $V_m$ which can lead to either SSI or FSI depending on other parameters of the system such as $R$, $C$ or $\omega_{z1}$.

While the previous routes were only carried out in a one-dimensional space, limiting the exploration of the dynamics, the definition of more complex routes,

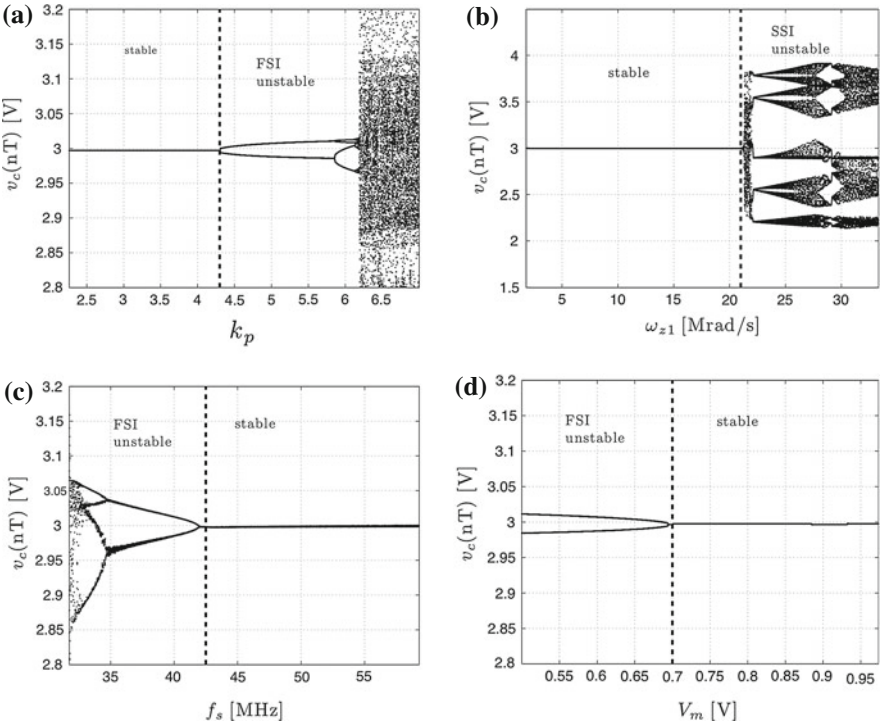


**Fig. 2.5** Bifurcation diagrams obtained by sweeping controller parameters. **a** Proportional gain $k_p$. **b** PI zero $\omega_{z1}$ and modulator parameters. **c** Switching frequency $f_s$ and **d** ramp amplitude $V_m$

depending on multiple swept parameters, allows characterizing the whole dynamic behavior in a more flexible way, such as the transition between different dynamics regimes and stability regions, which by exploring as a function of only one parameter can not be reached.

Therefore, given the $n$-dimensional design parameter space $W$, composed of $n$ parameters $p_i$ (for $i = 1$ to $n$), it is possible to define a route $\mathbf{v_y}(y)$ depending on only one variable $(y)$, which compresses the variation of other parameters $p_i$ into one route:

$$p_i = f_i(y) \quad \text{for } i = 1 \text{ to } n \tag{2.4}$$

$$\mathbf{v}_x(p_1, p_2, p_3, \ldots, p_n) = M \rightarrow \mathbf{v_y}(y) = \mathcal{P} \tag{2.5}$$

Note that different routes will be defined as a function of the parameter $\mathcal{P}$, namely constant level variable.

As a simple example, a linear route from SSI to FSI $\mathbf{v}_{\text{FS,SS}}^{\text{CCM}}$, shown in Fig. 2.6, is defined over the parametric space by the pair proportional gain-compensator zero $(k_p, \omega_{z1})$, with starting point (3, 25 Mrad/s) and end point (5, 10 Mrad/s). Therefore,

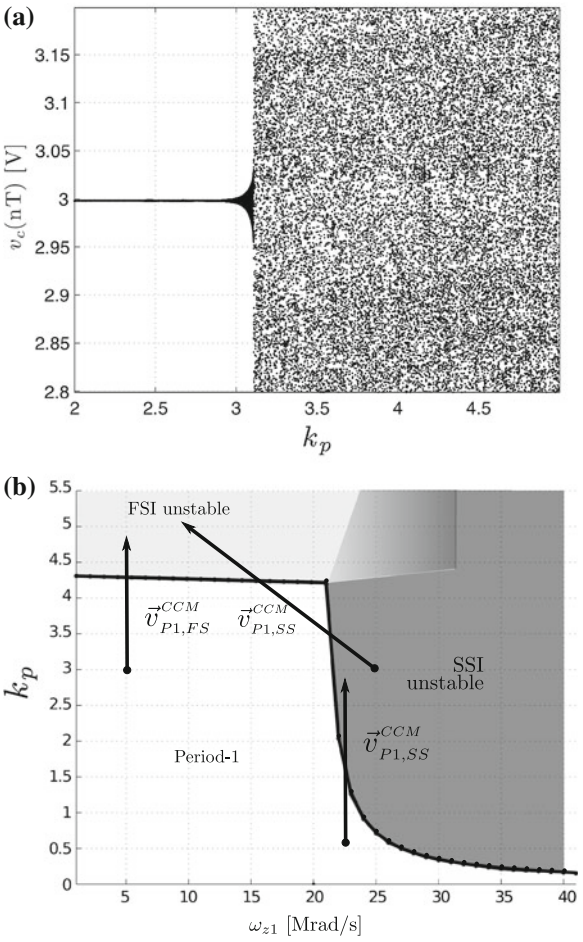


**Fig. 2.6** **a** Bifurcation diagram obtained by sweeping proportional gain $k_p$ with $\omega_{z1} = 21$ Mrad/s. **b** Stability boundary characterization over the space $(k_p, \omega_{z1})$ along with possible routes

under such condition, the route can be expressed as:

$$\mathbf{v}^{\mathrm{CCM}}_{\mathrm{FS,SS}} = f(k_p, w_{z1}) = \mathcal{P} \rightarrow k_p + \frac{2}{15}(\omega_{z1} 10^{-6} - 10) = \mathcal{P} \tag{2.6}$$

The route $\mathbf{v}^{\mathrm{CCM}}_{\mathrm{FS,SS}}(k_p, \omega_{z1})$ intends to explore the transition from FSI to SSI regions. Finally, the routes can be expressed only as a function of such variable $y$:

$$f(k_p, \omega_{z1}, P) \equiv f(y, \mathcal{P}) \tag{2.7}$$

in which each parameter can be expressed as a function of variable $y$:

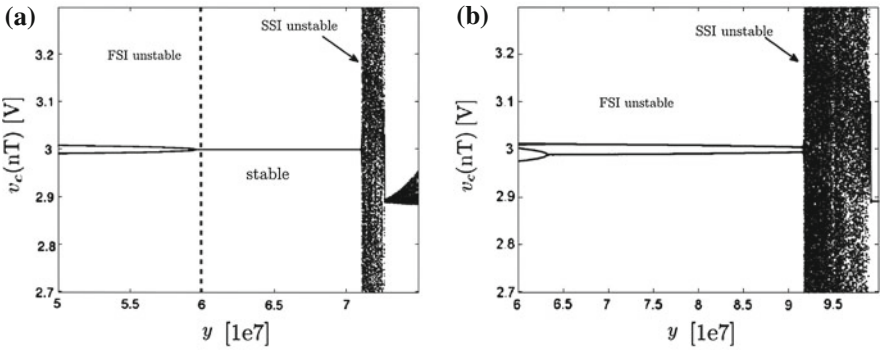


**Fig. 2.7** Route $\mathbf{v}_{\mathrm{FS,SS}}^{\mathrm{CCM}}$ by plotting the bifurcation diagram as a function of $y$. **a** $\mathcal{P} = 5$ and **b** $\mathcal{P} = 6$

$$\omega_{z1}(y) = y10^6 \tag{2.8}$$

$$k_p(y, \mathcal{P}) = \mathcal{P} - \frac{2}{15}(y - 10) \tag{2.9}$$

The route as a function of the variable $y$ is shown in Fig. 2.7, obtaining a bifurcation diagram that characterizes the transition between FSI and SSI regions. Note that the boundary is abrupt, without coexistence of attractors.

### *2.1.2 Dynamics in VMC Buck Converter Operating in DCM*

The next characterizations explore the effect of DCM upon the dynamic behavior, especially centered on the effect of crossing the boundary between both modes of the system. The parameters values used in this section are $V_g = 6\,\mathrm{V}$, $V_{ref} = 3\,\mathrm{V}$, $R = 6\,\Omega$, $L = 45\,\mathrm{nH}$, $C = 50\,\mathrm{nF}$, $f_s = 25\,\mathrm{MHz}$, $V_m = 1\,\mathrm{V}$, $k_p = 2.5$ and $\omega_{z1} = 1\,\mathrm{Mrad/s}$.

It is worth observing that having thoroughly explored the design parameter space in DCM, it has not been identified the exhibition of SSI. Then, considering only the existence of two behaviors in DCM, namely period-one and FSI, along with the abrupt nature of DCM boundary, the set of routes within the whole design parameter space and the dynamic analysis complexity is increased, as it is shown in the working regions in Fig. 2.8, depending on which parameters are swept.

Considering the boundary expression between the operating modes, shown in Eq. (2.3), the route from CCM to DCM is:

$$\mathbf{v}^{\mathrm{CCM,DCM}}(L,\, f_s,\, R,\, D) \tag{2.10}$$

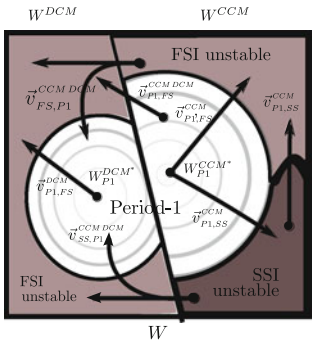


**Fig. 2.8** Descriptive working regions in DCM and CCM along with routes between modes and behaviors

The numerical simulation in Fig. 2.9 shows the effect of crossing from CCM to DCM considering different routes, obtained by sweeping different parameters and starting from different CCM conditions.

Different behaviors can be observed depending on which parameter is swept. The decrease of switching frequency may turn the converter into DCM and, once in DCM, it can lead to exhibit FSI in a similar way as it occurs in CCM. Regarding the inductance, the effect is opposite to its effect in CCM, since, as it is decreased, it cancels the period-doubling behavior once in DCM. Furthermore the effect of the load resistance on the SSI bifurcation is similar to the inductance since it also ends up canceling the instability once in DCM, firstly leading to FSI and subsequently leading to period-one behavior if it is decreased. Finally, it can also occur that crossing the conduction boundary from period-one in CCM leads to an abrupt jump into FSI, as it is shown by sweeping the voltage reference $V_{ref}$.

The effect of other parameters, which do not imply a change into DCM, such as the proportional gain $k_p$, are shown in Fig. 2.10 showing a similar effect as in the CCM case.

To summarize, we can observe that a VMC buck converter considering both conduction modes can be very complex, especially when the DCM is considered. This section has demonstrated that the different behaviors depend upon different parameters and that the same parameter can lead to different bifurcation scenarios depending upon the combination with other parameters of the multi-dimensional design parameter space. Furthermore, such complexity is increased when the route crosses the conduction mode boundary, which can lead to an abrupt transition in dynamics. While hitherto a qualitative characterization of the system behavior has been carried out focusing on pointing out the rich dynamic behavior of the switching power converter and exploring the effect of different nature parameters within the design parameter space, the next section is focused on a quantitative characterization of such dynamic behavior by establishing a set of power-oriented metrics that allow relating converter behavior properties to power application requirements for a given dynamic regime encountered in the design parameter space.

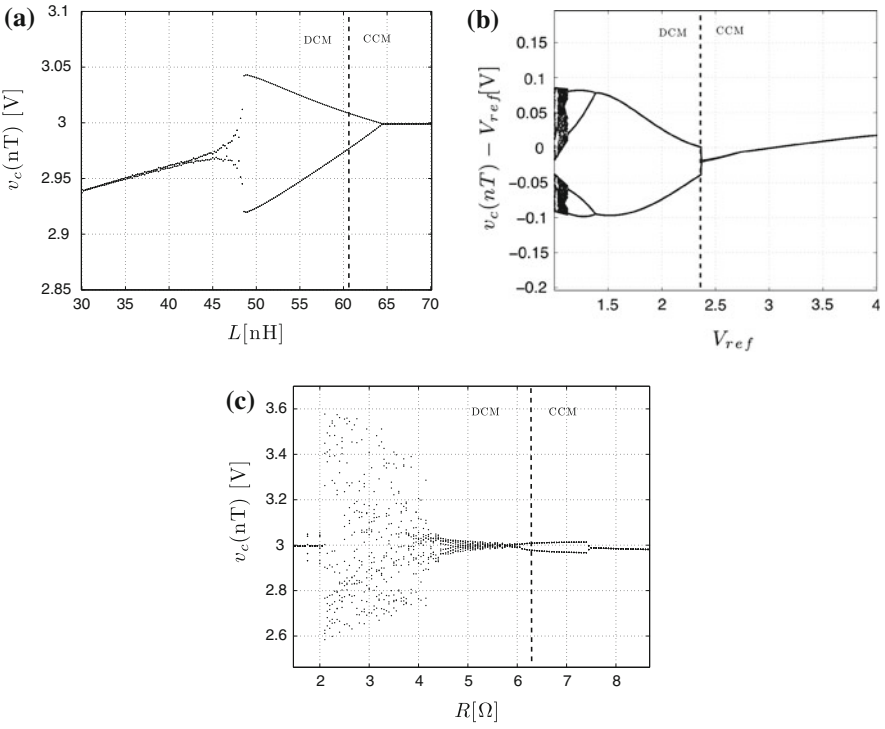


**Fig. 2.9** Different bifurcation diagrams obtained by crossing from CCM to DCM. **a** $\mathbf{v}_{\mathrm{FS,P1}}^{\mathrm{CCM,DCM}}(f_s)$ as a function of switching frequency $f_s$. **b** $\mathbf{v}_{\mathrm{FS,P1}}^{\mathrm{CCM,DCM}}(L)$ as a function of inductance $L$. **c** $\mathbf{v}_{\mathrm{P1,FS}}^{\mathrm{CCM,DCM}}(V_{ref})$ as a function of voltage reference $V_{ref}$ with $k_p = 2$. **d** $\mathbf{v}_{\mathrm{SS,P1}}^{\mathrm{CCM,DCM}}(R)$ as a function of output resistor $R$ and with $\omega_{z1} = 10\,\mathrm{Mrad/s}$

## 2.2 Power-Oriented Electrical Metrics Characterization of VMC Buck Converter Dynamics

This section is focused on a quantitative characterization of the instabilities that can be exhibited by a switching power converter, unveiling the impact they can have upon the system performances, with special attention on power-oriented electrical metrics, such as ripple, switching frequency or spectral behavior, which affect these performance.

Most of the previous works regarding the study of stability boundaries have been focused on predicting the exhibition of the different dynamic behaviors, but usually ignore evaluating the impact of such behaviors upon the system performance taking into account their final application. In such works, instabilities are analyzed from a qualitative standpoint, hence representing the bifurcation diagram or the state-plane, in which it is possible to observe the evolution of the state variables.

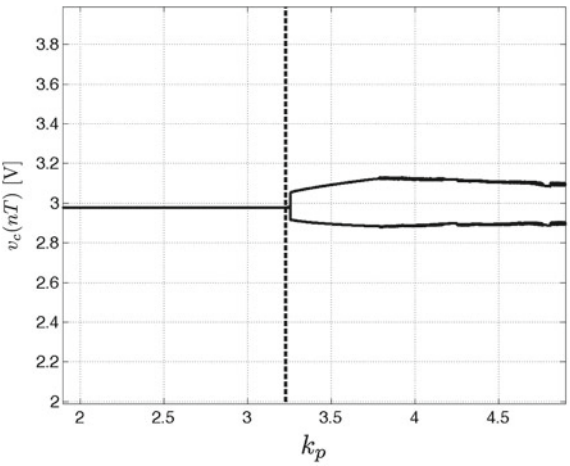


**Fig. 2.10** Bifurcation diagram by sweeping the proportional gain $k_p$

A complementary approach from an engineering standpoint, has been initially proposed in some works focusing on the effect of such instabilities in the spectrum (Banerjee et al. 2002; Deane and Hamill 1996; Giral et al. 2001; Woywode et al. 2003), in order to reduce electromagnetic interference of switching power converters. The idea is based on taking advantage of the well-known spread spectrum feature of chaotic behavior to reduce the harmonics at high frequencies.

However, the work presented in this section, addresses the characterization of the different instabilities not only on spectral performance, but also taking into account other power-oriented metrics, including output ripple and averaged switching frequency.

The fact that chaotic behavior can be exhibited requires to use a statistical tools, in a similar way as it has been done in (Woywode et al. 2003) in order to properly characterize the system. Therefore the chosen metrics are:

- The standard deviation of the output voltage waveform $\sigma_{v_c}$, in a steady-state period of time, as a measure of output ripple. Note that considering the average value 0, the RMS value coincides with the variance of the signal.
- The averaged switching frequency $\langle f_s \rangle$, understood as the average number of switching events per ramp period $T = 1/f_s$.

Note that while the previous characterization, in spectrum or state-variable is based on taking a photography under a given dynamic regime, the availability of such metrics allow to build an extended bifurcation diagram, showing the evolution of each metric by sweeping a given parameter of the parameter space.

The first exploration attempts to distinguish and compare the qualitative difference between both SSI and FSI. This is shown in Figs. 2.11 and 2.12 respectively.

In Fig. 2.11 the bifurcation diagram is shown by sweeping the proportional gain $k_p$, which ends up in chaotic behavior. The bifurcation diagram is complemented with the evolution plot of the averaged switching frequency $\langle f_s \rangle$ and standard deviation

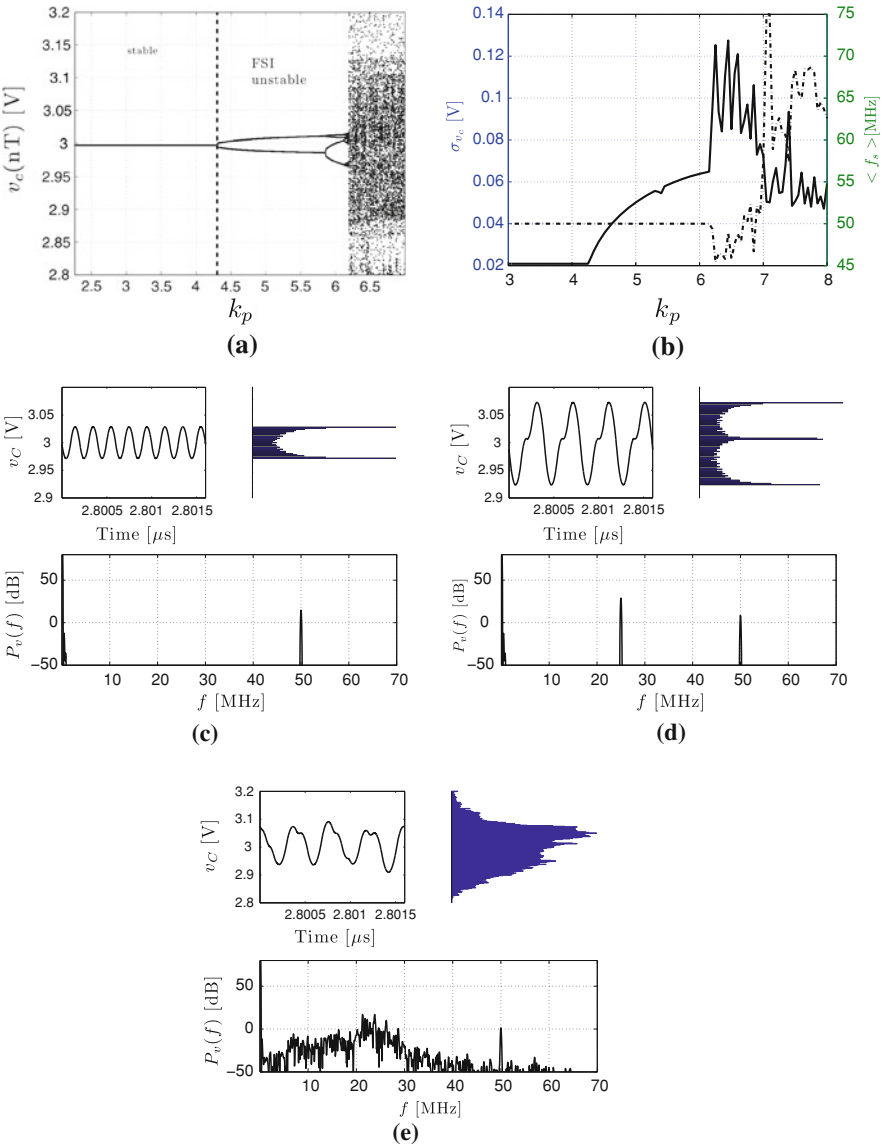


**Fig. 2.11** **a** Bifurcation diagram as function of $k_p$. **b** Standard deviation $\sigma_{v_c}$ (*solid*) and averaged switching frequency $\langle f_s \rangle$ (*dashed*). Representative time-domain waveform, histogram and spectrum (calculated within 1,000 periods) of the output voltage for **c** $k_p = 3$ (period-one). **d** $k_p = 5$ (period-doubling) and **e** $k_p = 7$ (chaotic regime) with $D = 0.5$

of output voltage $\sigma_{v_c}$. The exploration shows that when period-doubling is exhibited, the ripple steadily increases. Once into chaotic regime the ripple starts decreasing, but on the other hand the averaged switching increases. This can be understood because

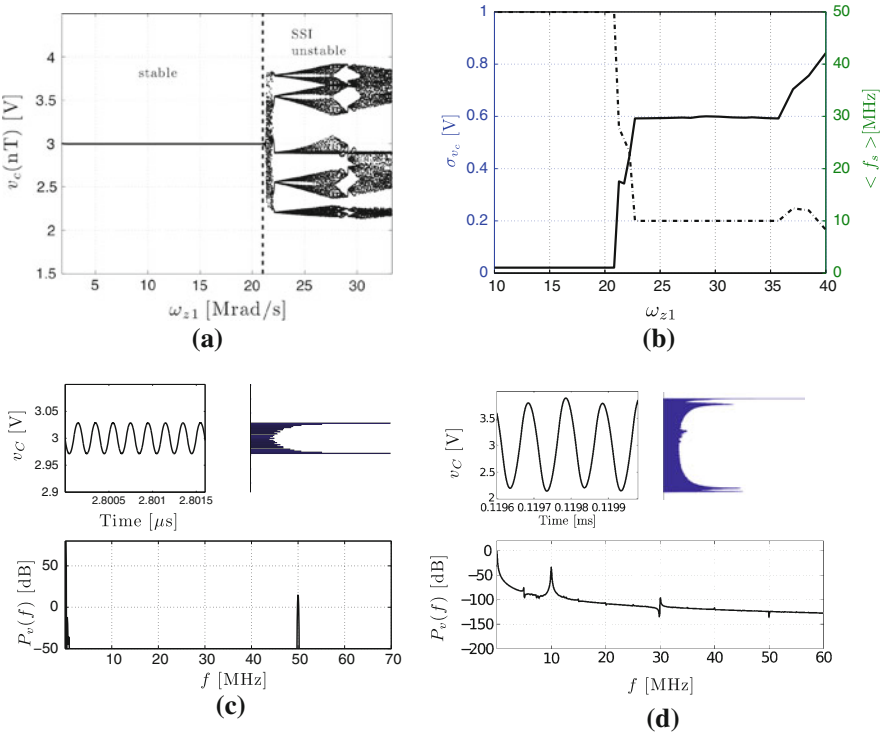


**Fig. 2.12** **a** Bifurcation diagram as function of $\omega_{z1}$. **b** Standard deviation $\sigma_{v_c}$ (*solid*) and average switching frequency (*dashed*) $\langle f_s \rangle$. Representative time-domain waveform, histogram and spectrum (calculated within 1,000 periods) of the output voltage for **c** $\omega_{z1} = 10$ Mrad/s (period-one) and **d** $\omega_{z1} = 25$ Mrad/s (SSI) with $D = 0.5$

of the exhibition of other instabilities (border collision) such as sliding behavior that entails multiple crossing of the ramp signal in one PWM ramp period. The spectrum of the different stages of the route to chaos entails the exhibition of subharmonics and, once into chaotic behavior, the well-known spread spectrum effect.

On the other hand, the effect of SSI into power metrics is different as it is possible to observe in Fig. 2.12. The exhibition of SSI leads to high reduction of the switching frequency and then a high increase in terms of ripple.

In addition, in Fig. 2.13 it is shown that the bifurcation diagram can vary depending upon the other parameters of the converter such as the duty cycle, which modifies the characteristic route of chaos: it is still composed of period-doubling exhibition, but it has different power metrics. Numerical simulations show that the averaged switching frequency is kept under the ramp frequency once within the chaotic regime and the ripple tends to decrease. This can be explained by the fact that being the duty cycle different of 0.5, the voltage applied to the inductor is unbalanced (in average) and this causes the system to exhibit skipping cycle phenomena hence reducing the number switching per cycle.

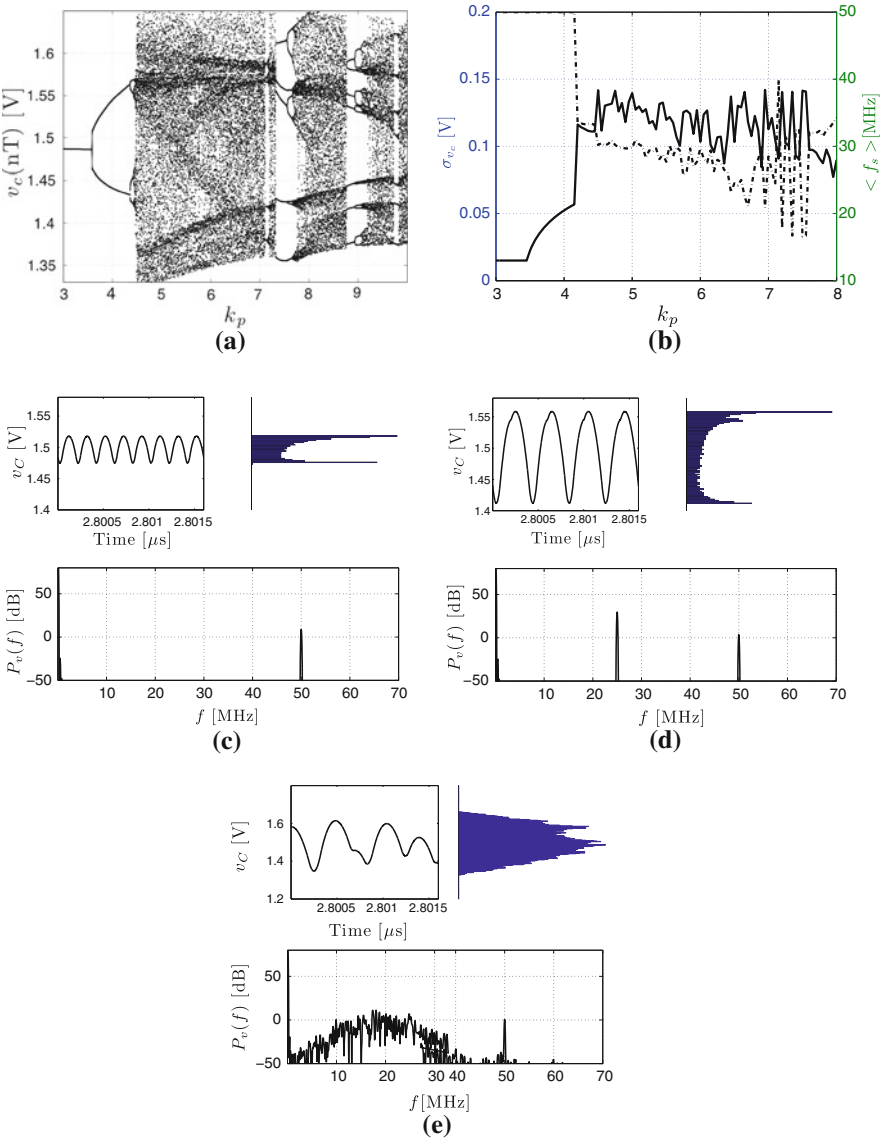


**Fig. 2.13** **a** Bifurcation diagram as a function of $k_p$. **b** Standard deviation $\sigma_{v_c}$ (*solid*) and average switching frequency $\langle f_s \rangle$ (*dashed*). Representative time-domain waveform, histogram and spectrum (calculated within 1,000 periods) of the output voltage for **c** $k_p = 3$ (period-one). **d** $k_p = 4$ (period-doubling) and **e** $k_p = 7$ (Chaotic behavior) with $D = 0.25$

## 2.3 Concluding Remarks

This chapter has focused on characterizing the different dynamic behaviors that a VMC buck converter with PI controller can exhibit. First, the chapter has identified the multidimensional design parameter space and characterized the dependencies of the stability boundaries upon the design parameter space. Numerical simulations based on the exact instantaneous state equations have shown rich and complex dynamic phenomena depending upon which parameter is swept. Furthermore, the chapter has discussed that trends towards miniaturization, namely reducing reactive components value or the switching frequency, can make the converter more prone to exhibit FSI, hence validating the interest on being able to predict such instabilities from a design-oriented standpoint and to synthesize improved dynamic controller. Finally, the chapter has quantified how the different dynamic regimes affect the switching converter from a power management perspective, by characterizing different power processing performance metrics such as the output voltage ripple (related to the quality of the DC–DC conversion), spectral behavior (related to EMI aspects) and average switching frequency (related to efficiency through the dominant switching losses).

http://www.springer.com/978-1-4614-2127-6

Chaos in Switching Converters for Power Management
Designing for Prediction and Control
Rodríguez Vilamitjana, E.; El Aroudi, A.; Alarcón, E.
2013, X, 178 p., Hardcover
ISBN: 978-1-4614-2127-6